Electronic Stopping of Heavy Ions in Solids *

Richard J. Mathar and Matthias Posselt
Institut für Ionenstrahlphysik und Materialforschung,
Forschungszentrum Rossendorf e.V., Postfach 510119, 01314 Dresden

1 Dec 1994

Abstract

One of the most fruitful theories in the field of the electronic energy loss of heavy ions in solids is the concept of effective charge theory. The familiar results have hitherto been based on the restricted target model of the homogeneous electron gas. The major part of the target characterization is added in form of experimental proton data, using the 'heavy ion scaling rule.' On the other hand, the more improved target model by Kaneko has only been used to calculate very light ion electronic stoppings up to now. To describe the physical processes from a more ab initio point of view, we propose the unification of this target model and effective charge theory. Refinements of the combined theory to overcome discrepancies with actual heavy ion stopping data are developed here.

1 Dielectric Theory of Electronic Stopping

1.1 The Model and the Lindhard-Winther Theory

The contribution of the excitation of target electrons to the ion stopping power is called electronic energy loss. In effective-charge theory the ion is a classical charge density $\rho_m(\mathbf{r}) = Z_1 e\delta(\mathbf{r}) + \rho_e(\mathbf{r})$ of a nucleus with atomic number Z_1 and a charge cloud ρ_e of bound electrons, moving with velocity $\mathbf{v}$ through the target material. The information on the target is exclusively taken from its dielectric function $\epsilon(k,\omega)$. Standard electrodynamics yields the induced polarization charge

$$\rho_p(\mathbf{k},\omega) = \rho_m(\mathbf{k},\omega)\left[\frac{1}{\epsilon(\mathbf{k},\omega)} - 1\right], \qquad (1)$$

where

$$\rho_m(k,\omega) = 2\pi\rho_m(k)\delta(\omega - \mathbf{kv}) \qquad (2)$$

is the Fourier transform of $\rho_m(\mathbf{r},t)$, and $\rho_m(\mathbf{k}) \equiv \int d^3r\, \exp(i\mathbf{kr})\rho_m(\mathbf{r})$ the ion form factor. Poisson's law yields the potential Φ_{ind} created by ρ_p, and its field $\mathbf{E}_{ind} = -\nabla\Phi_{ind}$. The energy transferred between $\mathbf{E}_{ind}$ and the ion determines the electronic stopping power $dE/dx = (dE/dt)/v$,

$$\frac{dE}{dt} = \mathbf{v}\int d^3r\, \rho_m(\mathbf{r})\mathbf{E}_{ind}(\mathbf{r})\,. \qquad (3)$$

In the case of homogeneous targets and spherical symmetric $\rho_m(\mathbf{r})$, it reduces to (SI units throughout) [2, 5, 13, 14]

$$\frac{dE}{dx} = \frac{1}{2\pi^2\epsilon_0 v^2}\int_0^\infty \frac{dk}{k}\,|\rho_m(k)|^2 \int_0^{kv} d\omega\,\omega\Im\left[\frac{1}{\epsilon(k,\omega)} - 1\right]. \qquad (4)$$

The Lindhard-Winther (LW) theory [13, 14] is furthermore restricted to (i) fully stripped ions, (ii) a homogeneous electron gas ('jellium') target with Fermi velocity v_F, (iii) its linear response, calculated (iv) within the lowest order perturbation theory, the so-called random phase approximation (RPA), and results in fig. 1. The RPA is the lowest order of the expansion of the polarization in terms of the one-electron radius $r_s \equiv \sqrt[3]{9\pi/4}v_0/v_F$, and becomes exact at high electron densities. However, the LW theory underestimates stopping powers in this limit, as a non-relativistic electron dispersion enters into the Lindhard dielectric function, and the electrons up to the surface of the Fermi sphere should stay non-relativistic [19].

*presented at the 'Arbeitstreffen des Verbundes *Festkörperphysik und Materialforschung mit nuklearen Methoden*,' 4 – 6 Oct 1994, Braunschweig, Germany

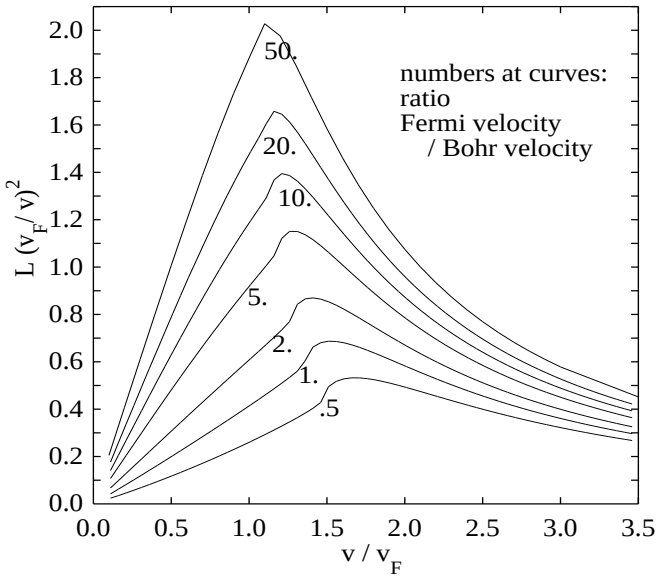

Figure 1: Lindhard-Winther stopping of point charges. $dE/dx = -8Z_1^2 k_F E_0 L \left(v_F/v\right)^2/(3\pi)$, where E_0 is 1 Ry, $k_F \equiv mv_F/\hbar$ and L the dimensionless Lindhard stopping number. Plasmons are excited, if v/v_F is approximately larger than $1+\sqrt[3]{v_0/(4\pi v_F)}$. The sharp bend there illustrates the 'equipartition rule' [5, 14]. The approximately linear dependence $dE/dx \propto v$ stems from $\Im\epsilon \propto \omega$ and $\Re\epsilon \approx$ const at small v, which means the underivative of the ω integral in (4) becomes $\propto \omega^3$ and the integral $\propto v^3$.

1.2 Effective Charge and Heavy Ion Scaling Rule

Fully stripped ions in arbitrary targets obey the scaling $dE/dx \propto Z_1^2$ according to eq. (4), if ϵ does not depend on Z_1, i.e., if we restrict to the linear electric susceptibility of the target [22, 25, 28]. But in the case of only partially stripped ions with extended clouds of bound electrons $\rho_m(k)$ is no longer $Z_1 e$. The deviation from the basic Z_1^2-scaling motivates the definition of the effective charge γZ_1 and effective-charge fraction γ [2, 16]

$$S(Z_1, v, q) \equiv (\gamma Z_1)^2 S(Z_1 = 1, v, q = 1)\,, \qquad (5)$$

where we have introduced the stopping cross section S per target atom, which is $|dE/dx|$ divided by the density of target atoms. Eq. (4) always predicts $q < \gamma < 1$; the effective charge is between the total ion charge $Qe = \int \rho_m(\mathbf{r}) d^3r$ and the nucleus charge $Z_1 e$. The integration over k, which represents the momentum exchange, may be interpreted as a addition of contributions of target electrons with small impact parameter (close, hard collisions) that feel more of the unscreened nucleus charge, and with large impact parameter (distant, soft collisions) that see the screened charge Qe.

In the current practise of heavy ion stopping calculations [2, 29, 30] eq. (5) is not interpreted as a mere definition, but as the 'heavy ion scaling rule.' The dependence of γ on q, the target atomic number Z_2 and v is estimated from a jellium target model. Experimental proton data $S(Z_1 = 1, v, q = 1)$ and γ are inserted into the rhs of (5) to compute the heavy ion stopping. This scaling step becomes necessary to incorporate the full information on the target polarizability, which is absent in the theoretical estimates of γ. The experimental proton data deliver the contributions of the target inner shell electrons, whereas γ is parametrized by v_F and bears only information on the free and valence target electrons. Fig. 2 illustrates the amount of information provided by the proton data.

The motivation of our work is to present a more ab initio stopping power calculation by using (4) directly, which can only be achieved by installing an improved target description. The heuristic scaling step is intended to become obsolete.

2 The Kaneko Theory of Target Shells

We make use of the Kaneko theory of superimposed target shells [8–10] which

- □ supplies a parametrization of *all* elemental targets, shell by shell,
- □ has been proven to succeed in the prediction of proton data, and
- □ supports the numerical evaluation by giving analytical expressions to the susceptibility of each target shell.

The theory calculates the stopping cross section per target atom by the independent superposition of the 1s, 2s, 2p, ... shell cross sections, and, when appropriate, of a 'shell'

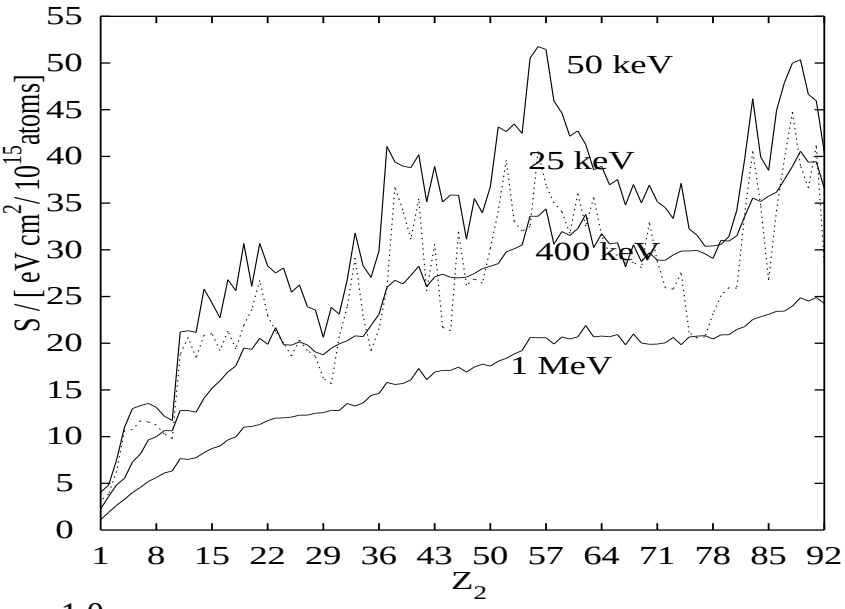

Figure 2: Z_2 oscillations of proton electronic stopping cross sections at four different proton energies ('scoef'-data file by [29]).

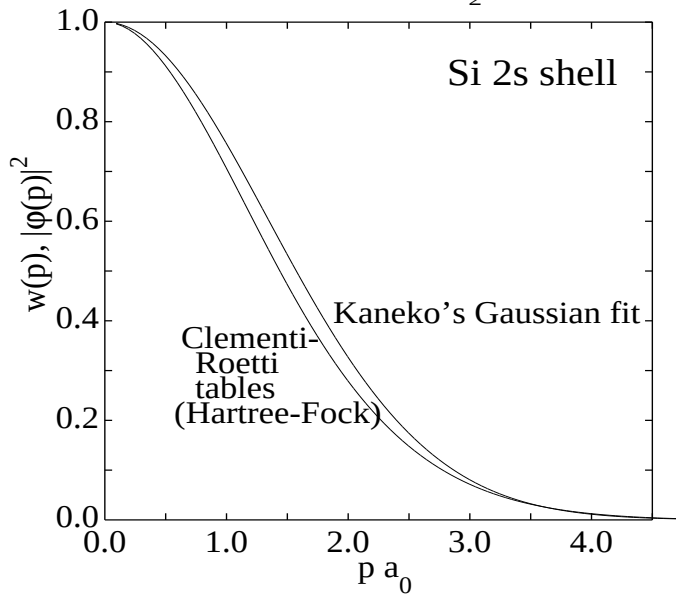

Figure 3: Momentum distribution $w(p)$ of the Si 2s shell with the Gaussian approximation ($\bar{q}_1 a_0 = 1.89$) and the value $|\varphi(p)|^2$ obtained from the Fourier transform of the Roothaan-Hartree-Fock result (extended basis) of [3]. Both are standardized to coincide at $p = 0$.

of free electrons. The dielectric function of the latter is taken as in the LW theory.

$$S = \sum_{\text{bnd,free}} S_{\text{shell}} \cdot \tag{6}$$

This assumption of independence is similar to the Bragg's rule of the ion stopping in compound targets [31] or to the Matthiesen's rule of the scattering probability of electrons due to (non)ionized impurities and phonon branches in semiconductors. It means that the polarization charges of the shells are added, and each one is calculated as if the excitation was induced solely by the field of the ion. The linear Maxwell equations add the induced fields and stopping powers to give (6). A more precise description might control the polarization of each shell by the influence of the ion field *and* the remaining shells, i.e., insert the retarded susceptibilities χ^R into

$$\epsilon = 1 + \sum_{\text{free,bnd}} \chi^R \tag{7}$$

and in (4). (We write χ^R for the susceptibilities and χ for the density parameters, and drop the index 'shell' for brevity.) This procedure diminishes the polarization charges and stopping powers, because each shell is excited by the ion field already screened by the polarization charges of the remaining shells. We shall only present results from (6), not from (7) here.

The susceptibility χ^R of each target shell of bound electrons was calculated in the RPA, modelling the electrons by a wave packet with a Gaussian momentum distribution

shell	Mg ^{1}S		Si ^{3}P		Fe ^{5}D		Fe ^{3}F	Co ^{4}F	Ni ^{3}F	Cu ^{2}S	
	d	e	d	e	d	e	e	e	e	d	e
1s	6.687	6.788	7.872	7.989	14.97	15.25	15.26	15.83	16.39	16.77	17.01
2s	1.518	1.496	1.906	1.890	4.089	4.166	4.172	4.250	4.429	4.625	4.589
3s	(0.3337	0.3344)	(0.501	0.499)	1.406	1.410	1.413	1.473	1.532	1.584	1.582
4s					(0.3365	0.3354)	(0.3376)	(0.3442)	(0.3493)	(0.3125	0.3151)
2p	1.421	1.378	1.839	1.797	4.269	4.227	4.228	4.429	4.617	4.856	4.809
3p			(0.3932	0.3833)	1.266	1.262	1.265	1.328	1.390	1.436	1.426
3d					0.9629	0.8447	0.8229	0.8837	0.9272	1.035	0.8649

Table 1: Values of $\bar{q}_1 a_0$ by the less accurate 'double zeta' functions (column header 'd') and the functions by the extended basis (header 'e') of [3] in (15). The tables [10] cite 'double zeta' values for Mg, Fe and Cu and extended basis values for Si. Numbers in parentheses are not used for solid targets — the respective shells are replaced by the LW model.

in the ground state,

$$w(p) = \exp\left\{-\left(p/\bar{q}\right)^2\right\} \qquad , \tag{8}$$

$$\Im\chi^R(k,\omega) = -\frac{e^2}{4\pi^2\hbar k^2\epsilon_0}\int d^3p\ \left(w(\mathbf{p}+\mathbf{k}) - w(\mathbf{p})\right) \times\delta\left(\omega - \frac{\hbar(\mathbf{p}+\mathbf{k})^2}{2m} + \frac{\hbar\mathbf{p}^2}{2m}\right) \tag{9}$$

$$= \frac{\pi\chi^2}{8z^3}\left[\exp\{-(u-z)^2\} - \exp\{-(u+z)^2\}\right], \tag{10}$$

where the 'Lindhard variables' are $z \equiv k/(2\bar{q})$, $u \equiv m\omega/(\hbar\bar{q}k)$, the squared density parameter is $\chi^2 \equiv 1/(\pi\bar{q}a_0)$ and a_0 the Bohr radius. A subsequent Kramers-Kronig (KK) analysis gave $\Re\chi^R$,

$$\Re\chi^R(z,u') = -\frac{P}{\pi}\int_{-\infty}^{\infty}\frac{\Im\chi^R(z,u)}{u'-u}du \tag{11}$$

in terms of confluent hypergeometric functions (case $l = 0$ in appendix B). The resulting $\epsilon = 1 + \chi^R$ was inserted shell by shell into

$$S_{\text{bnd}} = \frac{-2N_{\text{bnd}}}{\sqrt{\pi}\epsilon_0 v^2\bar{q}^3}\int_0^\infty\frac{dk}{k}\left|\rho_m(k)\right|^2\int_0^{kv}d\omega\omega\Im\left[\frac{1}{\epsilon(k,\omega)} - 1\right] \tag{12}$$

$$= \frac{Z_1^2 e^4}{4\pi\epsilon_0^2 m v^2}N_{\text{bnd}}L_{\text{bnd}}(v); \tag{13}$$

$$L_{\text{bnd}} \equiv -\frac{8}{\pi^{3/2}\chi^2}\int_0^\infty dz z\left|\frac{\rho_m(z)}{Z_1 e}\right|^2\int_0^{v/\bar{v}}duu\Im\frac{1}{\epsilon(z,u)}; \tag{14}$$

$$(\bar{v} \equiv \frac{\hbar\bar{q}}{m} \quad \text{and} \quad \sum_{\text{bnd,free}} N_{\text{shell}} = Z_2).$$

The characteristic momentum $\bar{q}$ of the wave packet of each shell was deduced via

$$\bar{q} = N_{\text{bnd}}^{1/3}\bar{q}_1 \quad ; \quad \bar{q}_1 = 2\sqrt{\pi}\left|\int d^3r\,\varphi(\mathbf{r})\right|^{-2/3} \tag{15}$$

from the wave function $\varphi(\mathbf{r})$ of free-atom Roothaan-Hartree-Fock calculations [3, 18]. To check the validity of this one-parametric approximation to the momentum distribution, fig. 3 shows a comparison with $\left|\varphi(p)\right|^2$. An increase of $\bar{q}$ takes the same influence on the shell contribution to the stopping power as an increase of k_F on the free-electron contribution: a shift of the maximum of $S(v)$ towards higher energies.

Though the individual values of $\bar{q}$ are not at all free parameters, some uncertainty arises from the usage of either the 'double zeta' functions, or the functions with the 'extended' basis set of the Clementi-Roetti (CR) tables[3] in (15). Selected examples are listed in table 1. We may obtain even more rough and quick estimates, if φ is approximated by one single orbital $\propto r^{n-1}e^{-\zeta r}$ with principal quantum number n — the coefficient ζ may e.g. be taken from the 'single zeta' values with the expansion coefficient near to ±1 in [3]. The Fourier transforms of these Slater Type Orbitals are [1]

$$\int d^3r\, e^{i\mathbf{qr}}r^{n-1}e^{-\zeta r}Y_{lm}(\mathbf{r}) =$$

$$2^{n+2}\pi(n-l)!(iq)^l\zeta^{n-l}\sum_{j=0}^{[(n-l)/2]}\frac{\omega_j^{nl}}{(q^2+\zeta^2)^{n+1-j}}Y_{lm}(\mathbf{q}), \tag{16}$$

with $\omega_j^{nl} \equiv (-1/[4\zeta^2])^j(n-j)!/[j!(n-l-2j)!]$. The spherical harmonics Y_{lm} depend only on the directions of their arguments. Using (16) in (15) for the 'single zeta' approximation, the width of the momentum distribution is $\bar{q}_1 = \frac{1}{2}\pi^{1/6}\zeta$ if $n = 1$, $\bar{q}_1 = \frac{1}{2}3^{-1/3}\pi^{1/6}\zeta$ if $n = 2$, and $\bar{q}_1 = 2^{-8/3}5^{1/3}\pi^{1/6}\zeta$ if $n = 3$. It relates to the atomic size parameter as expected from the uncertainty principle.

3 Excitation Gaps of Inner Target Shells

Examples of proton data obtained from the original Kaneko theory show good general agreement with the experimental values (fig. 4).

In the high-velocity region, it generally overestimates the stopping power by roughly 5 – 10 %. This is an unsatisfactory feature, as the parameter set of the shells should at least reach the accuracy of the Bethe theory there. We suppose that this overestimation is created by an overestimation of the energy loss function, since the integral (10) had been computed allowing the electrons to be scattered by *any* wavenumber and energy. Actually, excitations with energy transfer $\hbar\omega$ less than the binding energy E_{bnd}, which means scattering into band gaps or occupied states, are forbidden and cannot contribute to the polarization. The values of E_{bnd} should represent the minimum energy difference of the individual energy level of the shell and the next upper empty or non-filled band. In practise, we approximated the values E_{bnd} by the energy difference between the individual shell and the level of the highest occupied orbital of the target atom, taken from the CR tables. In so far, the band widths and band dispersion of the solids have been neglected in favour of a simple atomic model.

We propose a correction 'by hand' and cut $\Im\chi^R$ of the Kaneko theory by the substitution

$$\Im\chi^R(k,\omega) = 0, \quad \text{if} \quad |\hbar\omega| < E_{\text{bnd}} \qquad , \tag{17}$$

or, in terms of the Lindhard variables

$$\Im\chi^R(u,z) = 0, \quad \text{if} \quad uz < \frac{1}{2}\left(\pi\chi^2\right)^2 \frac{E_{\text{bnd}}}{2E_0}. \tag{18}$$

No correction is introduced to the values if $|\hbar\omega| > E_{\text{bnd}}$, or to shells of free electrons in solids. This change of $\Im\chi^R$ should be accompanied by a reanalysis of $\Re\chi^R$ by (11), which is no longer known in analytical form. It would demand another time-consuming numerical integration in (14). Instead, the subsequent figures have been obtained with the original values of $\Re\chi^R$ inserted into $-\Im(1/\epsilon) = \Im\epsilon/\left(\Re^2\epsilon + \Im^2\epsilon\right)$ and (14). To control the induced error, the values of $\Im(1/\epsilon)$ with the reanalysed and original $\Re\chi^R$ are compared in fig. 5 for one example. It proves that the differences are small and constrained to small areas nearby $\hbar\omega \approx E_{\text{bnd}}$, the bold hyperbola. Including the KK analysis would result in a slight reduction of the integrand near the plasmon ridge and a further reduction of the stopping cross section.

The Kaneko theory defines a plasmon energy $\hbar\omega_p$ of each shell [9]

$$\hbar\omega_p = 2E_0/(\pi^{7/4}\chi^3)$$

and the plasmon dispersion relation

$$u^2 \approx \sqrt{\pi}\chi^2/(4z^2) + 3/2 + z^2 \qquad .$$

In fig. 5 this plasmon ridge is seen in the upper left corner and inside the region which is retained by the energy cut. In the sense of the simple criterion $E_{\text{bnd}} > \hbar\omega_p$, the energy cut suppresses the plasmon excitation of all s shells, of the 2p shells of target elements heavier than ('beyond') $_{14}$Si, of the 3p shells beyond $_{25}$Mn, of the 4p shells beyond $_{42}$Mo, of the 5p shells beyond $_{56}$Ba and of the 3d shells beyond $_{43}$Tc.

Results of this energy cut are given in fig. 4. The high-energy tail of the theory is improved and matches the fit to the proton data by Ziegler, Biersack and Littmark (ZBL) with winning accuracy. Another difference to the original theory is that the stopping cross sections of the energy-cut shells of bound target electrons are no longer $\propto v$ at low velocities but rise with a higher power of v [6, 26]. At low velocities, the total cross section has become worse than the original theory by the reduction of the bound-shell contributions. This remaining underestimation of the stopping is a well-known systematic feature of the RPA and of the neglect of nonlinear susceptibilities applied to the free electron gas [15, 20, 21, 23].

The energy cut will always be tacitly included in the subsequent calculations.

4 Electronic Stopping of Heavy Ions in Kaneko's Targets, the Dead Sphere

The straight forward step now is the usage of form factors $\rho_m(k)$ of partially stripped heavy ions. (The term 'heavy' does not refer to the ion mass directly — the ion mass does not enter into (4).) To meet the problem of installing an ion model and its respective stripping degree q [17, 28] we shall (i) use the Brandt-Kitagawa (BK) ion model [2]

$$\rho_e(r) = \frac{-Ne}{4\pi\Lambda^2}\frac{e^{-r/\Lambda}}{r}\,;\; \rho_m(k) = Z_1 e\frac{q + (k\Lambda)^2}{1 + (k\Lambda)^2} \tag{19}$$

to describe the ion with $N \equiv Z_1 - Q$ bound electrons and size parameter Λ, and (ii) take the charge fraction q and Λ from the ZBL [29] programme. The advantage of this procedure is the approximate incorporation of the knowledge on the ion shell structure (fig. 6), and the related Z_1 oscillations.

Because q and Λ were determined in a joint fit to experimental data [29], potentially artificial features of one of

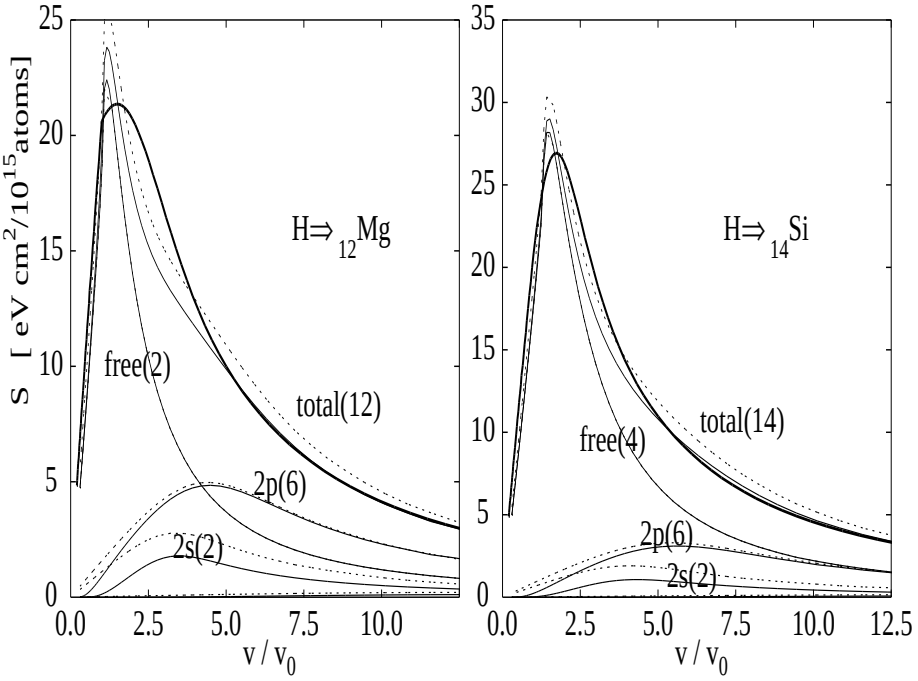

Figure 4: Proton stopping cross sections S and S_{shell} in $_{12}$Mg and $_{14}$Si targets. Dotted lines: Original Kaneko theory. Bold lines: ZBL [29]. Thin lines: results with the following cut energies E_{bnd} (in a.u.): Mg 1s 48.78, Mg 2s 3.515, Mg 2p 2.029, Si 1s 68.52, Si 2s 5.859, Si 2p 3.959, free none. The contributions of the target 2s shells are reduced most effectively by the energy cut (17). Numbers in parentheses denote N_{shell}.

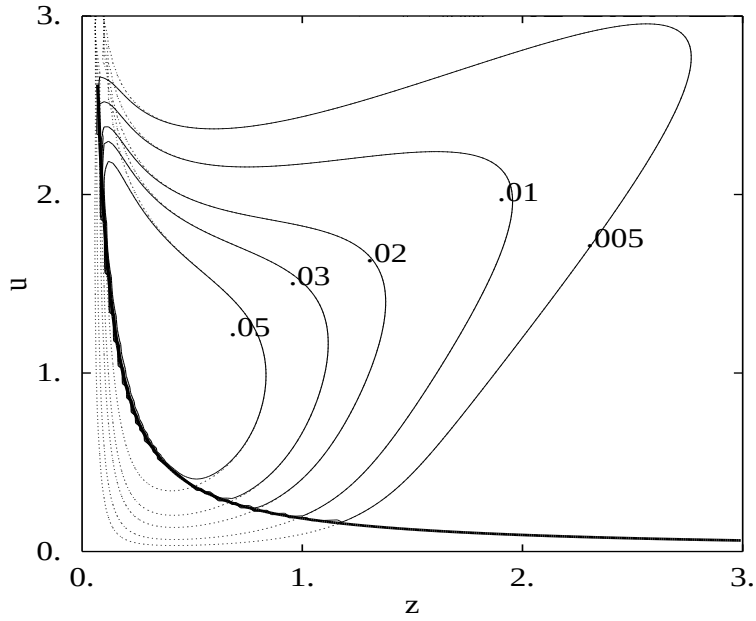

Figure 5: Contour plots of $-z\Im[1/\epsilon(z,u)]$ with the parameters of the Si 2p shell: $\bar{q}_1 a_0 = 1.797$, $E_{\text{bnd}} = 3.959$ a.u. and $N_{\text{shell}} = 6$. A corresponding graph for a homogeneous Fermi gas is eg [14, Fig. 1]. The bold hyperbola is defined by (18). The energy cut sets the values below and left from it to zero. Solid lines are calculated using (18) with the KK reanalysis included. The dotted lines without KK reanalysis of $\Re\chi^R$ were used in all subsequent calculations.

them are expected to be moderated by using both at one time. The disadvantage is that they were bound to the correctness of a fit formula $\gamma(k_F)$ that we shall implicitly replace by using (4) for protons *and* heavy ions. If the results of this ion model combined with the Kaneko target model fail to reproduce the experimental values for a common effective velocity $v/(v_0 Z_1^{2/3})$, one should attribute it rather to a misfit of q than to another systematic incompleteness of the combined theory presented here.

The thin solid curves in fig. 7 illustrate that, increasing Z_1, the stopping cross sections predicted by the theory become worse more and more, which is most pronounced at the maxima of $S(v)$.

This might have caused people either to study ions only up to $_3$Li, or to restrict its usage to $v < v_0$ and import effective charges actually from a combined scattering phase method and BK theory [11, 27]. Our suggestion in this section — now affecting all kinds of target models of effective charge theory — serves to explain and remove this discrepancy. We regard the polarization charge ρ_p (1) to

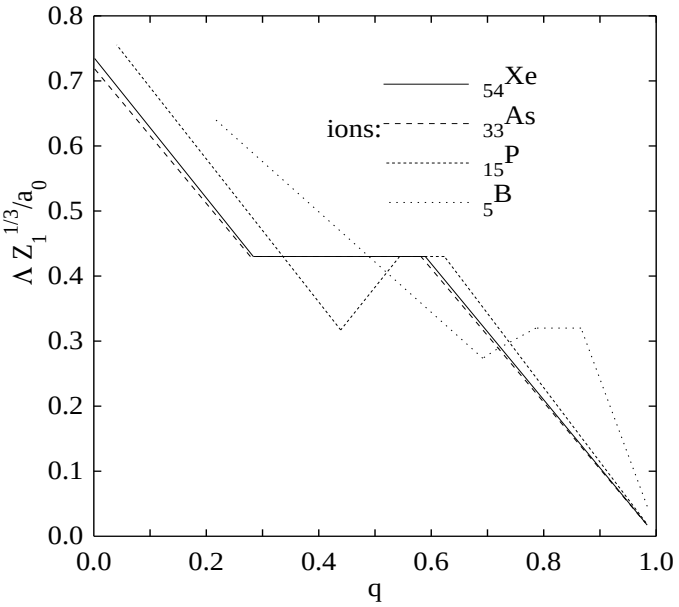

Figure 6: Scaled ion size parameters Λ by ZBL [29]. The tabulated Z_1 correction factor is already included. The scaling $\propto Z_1^{-1/3}$ is predicted by statistical ion models [2]. The absolute value of Λ is generally smaller for heavier ions. The lines are practically independent from Z_2. The upper left endings mark the values of $v = 0$, i.e., light ions are assumed to be partially ionized even at rest.

be absent in a sphere of radius r_c located at the ion nucleus

$$\Phi_{ind}(\mathbf{r},t) = \frac{1}{4\pi\epsilon_0}\int_{|\mathbf{r}'-\mathbf{v}t|>r_c} d^3r'\,\frac{\rho_p(\mathbf{r}',t)}{|\mathbf{r}-\mathbf{r}'|}, \qquad (20)$$

and call it a 'dead sphere' analogous to the model of a dead layer of the excitonic polarization near a semiconductor surface (cf. [24, Sec. 5]). The physical idea is to exclude the excitation of target electrons in the close neighbourhood of the ion nucleus, where the bound electrons occupy the available space and provide already a good description of the electron density. The jellium model of an infinitely extended positive background and homogeneous density of target electrons is replaced inside the sphere by the results of an atomic theory for the ion. The model removes the contributions of two processes to the polarization that actually do not happen, (i) either a target electron being scattered from outside into the close neighbourhood of the nucleus or (ii) a target electron nearby the nucleus being scattered to the outside. In this picture, the ion itself is polarized by the field $\mathbf{E}_{ind}$; the classical description would mean a shift of the bound electrons relative to the nucleus, the quantum mechanical the Stark effect. This 'internal' charge separation cannot exert a net force on the ion directly, i.e., does not contribute to the stopping power in the order $S \propto Z_1^2$.

The computation of the new stopping power is deported to appendix A. The best fit of r_c to improve the theoretical stopping cross section is in the order of the size parameter Λ (fig. 7), which is a function of the ion velocity and stripping degree (fig. 6). It indicates that the physical picture of a non-polarizable core region around the ion nucleus is correct. In the case of $_{15}$P, r_c is comparable with the radius of the L shell ($0.36a_0$ in the sense of the maximum of $4\pi r^2|\varphi(r)|^2$) at $v \approx 0$, and tends towards the radius of the K shell ($0.07a_0$), if only two bound electrons are left. In the case of $_{33}$As, r_c is approximately the radius of the M shell ($0.50a_0$) and tends towards the radius of the L shell ($0.15a_0$), if Q approaches 23. In the case of $_5$B, however, the best result is obtained without dead sphere. But this looks reasonable, too, because at $v > 2v_0$ only two bound electrons are left. The density of these $N \approx 2$ electrons is no longer much larger than the density of the target electrons, their 'repelling effect' too small and localization too weak to prevent a penetration and overlap of target electrons.

The sudden cut of the polarization charge at some distance r_c from the ion nucleus is a rather artificial model and has been chosen to allow the analytical treatment of an intermediate integral in appendix A. It may produce artificial oscillations in wave number space. Future work should try smoother transient functions for the polarization and include hydrogenlike ion electron densities, which are more appropriate to light ions than the BK form (19).

5 Susceptibilities of p and d Subshells

Our final proposal returns to the target polarization and wishes to find out, whether the left-shift of the maximum of the theoretical stopping data of heavy ions (eg As in fig. 7) with respect to v compared with ZBL suggests an-

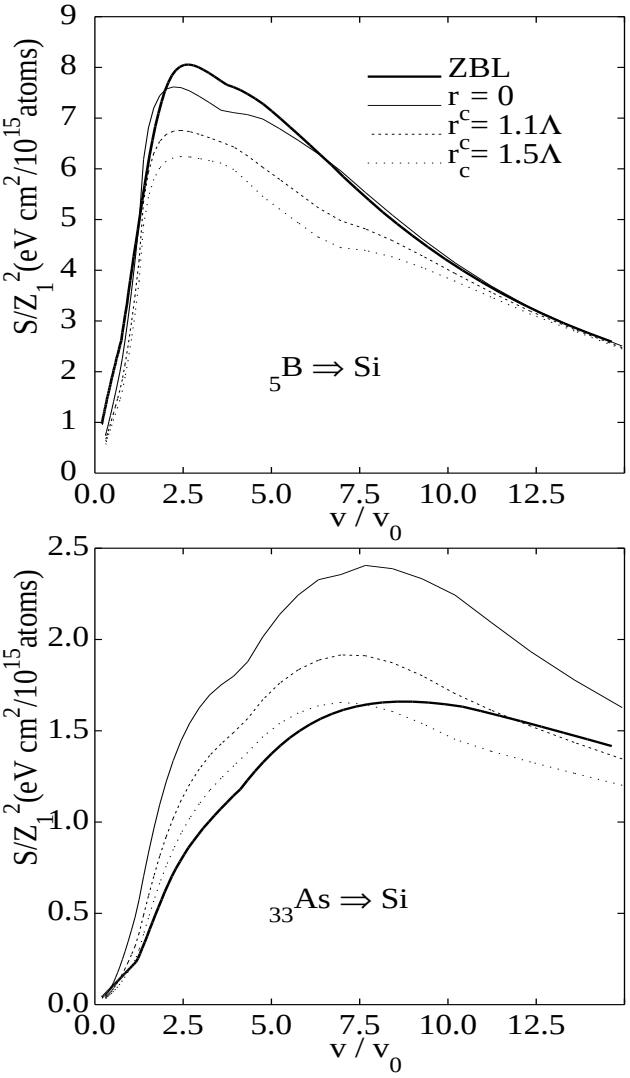

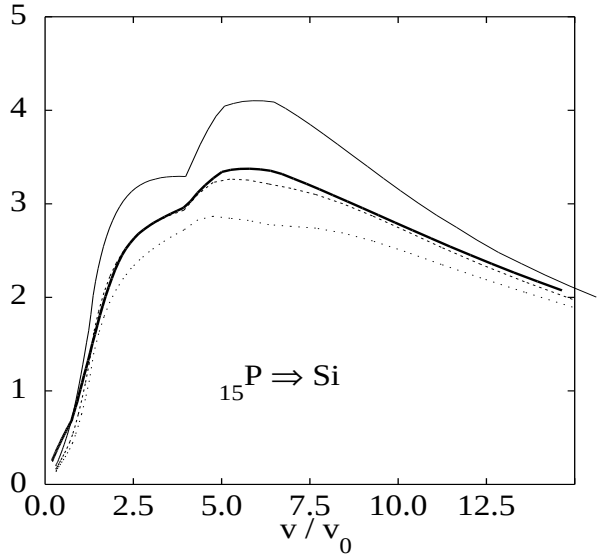

Figure 7: Total electronic stopping cross sections of ZBL (thick line), and of the Kaneko theory (energy cut as in fig. 4) with three different choices of the 'dead sphere' radius r_c relative to the size parameter Λ, obtained by (26). The choice $r_c = 1.1\Lambda$ for $_{15}$P means $r_c \approx 0.33a_0$ at $v = 0$ ($Q = 0$), $r_c \approx 0.19a_0$ at $v = 5v_0$ ($Q \approx 7.6$), $r_c \approx 0.11a_0$ at $v = 10v_0$ ($Q \approx 11.5$) and $r_c \approx 0.055a_0$ at $v = 15v_0$ ($Q \approx 13.3$). The choice $r_c = 1.5\Lambda$ for $_{33}$As means $r_c \approx 0.34a_0$ at $v = 0$ ($Q = 0$), $r_c \approx 0.2a_0$ at $v = 5v_0$ ($Q \approx 10.5$) and $r_c \approx 0.13a_0$ at $v = 15v_0$ ($Q \approx 24$). The form function (19) implies that 30% of the N bound electrons are inside a sphere of radius 1.1Λ and 44% inside the radius 1.5Λ around the ion nucleus. (The kinks originate from the steps of the ion size shown in fig. 6 for the same ion species.)

other weakness of the model. The maximum of $S(v)$ of light ions is predicted accurately in the Kaneko model, and is determined by the free target electrons. As Z_1 increases, its position is generally fixed by the next inner p and d shells. We shall present a reason to change the treatment of these subshells with nonzero angular momentum quantum number. The Gaussian approximation (8) of the momentum distribution was derived from an interesting application of thermodynamics [9]. Subsequently it is directly interpreted in the sense of wave functions in momentum space. Nearly Gaussian forms of $|\varphi(\mathbf{k})|^2$ are obtained for any angular momentum quantum number l, if the wave function $\varphi(\mathbf{r})$ is averaged over all directions of $\mathbf{r}$, equivalent to replacing the angular dependence $\propto Y_{lm}(\mathbf{r})$ by the constant $\propto Y_{00}(\mathbf{r})$, prior to the Fourier transform (16). Our calculation means switching to the momentum representation first, and averaging afterwards across $\mathbf{p}$, replacing $Y_{lm}(\mathbf{p})$ by $Y_{00}(\mathbf{p})$. The factor $(iq)^l$ in (16) recommends the generalized ansatz

$$w(p) = c_l^2 p^{2l} \exp\left\{-\left(p/\bar{q}\right)^2\right\} \qquad (21)$$

that leaves the free-electron and s target shells unchanged. The standardization factors c_l are chosen to conserve the total probability of finding the electrons with any wave number p which is already used in the original theory

$$\int d^3p\, w(p) = c_l^2 \pi^{3/2} (2l+1)!! 2^{-l} \bar{q}^{2l+3} \stackrel{!}{=} \pi^{3/2} \bar{q}^3$$

$$\Rightarrow \qquad c_l^2 = \begin{cases} 1 & l = 0 \text{ (s shell)} \\ 2/(3\bar{q}^2) & l = 1 \text{ (p shell)} \\ 4/(15\bar{q}^4) & l = 2 \text{ (d shell)} \end{cases} . \qquad (22)$$

It is equivalent to retaining the quantity $\int d^3r |\varphi(r)|^2$ of the original theory. The calculation of the linear susceptibility within the RPA is presented in appendix B and delivers analytical expressions again. The appropriate fit values to $\bar{q}_1$ have been chosen to let the wave number p_m

shell	Mg 1S	Si 3P	Fe 5D	Co 4F	Ni 3F	Cu 2S
2p	1.592	2.048	4.514	4.783	4.980	5.174
3p		(0.6069)	1.135	1.197	1.248	1.267
3d			0.8918	0.9197	0.9588	0.8373

Table 2: Values of $\bar{q}_1$ by the extended basis of [3] in (23). Values for s shells stay as in table 1. Again, the number in parentheses is not used for solid targets, but the respective shell replaced by the LW model.

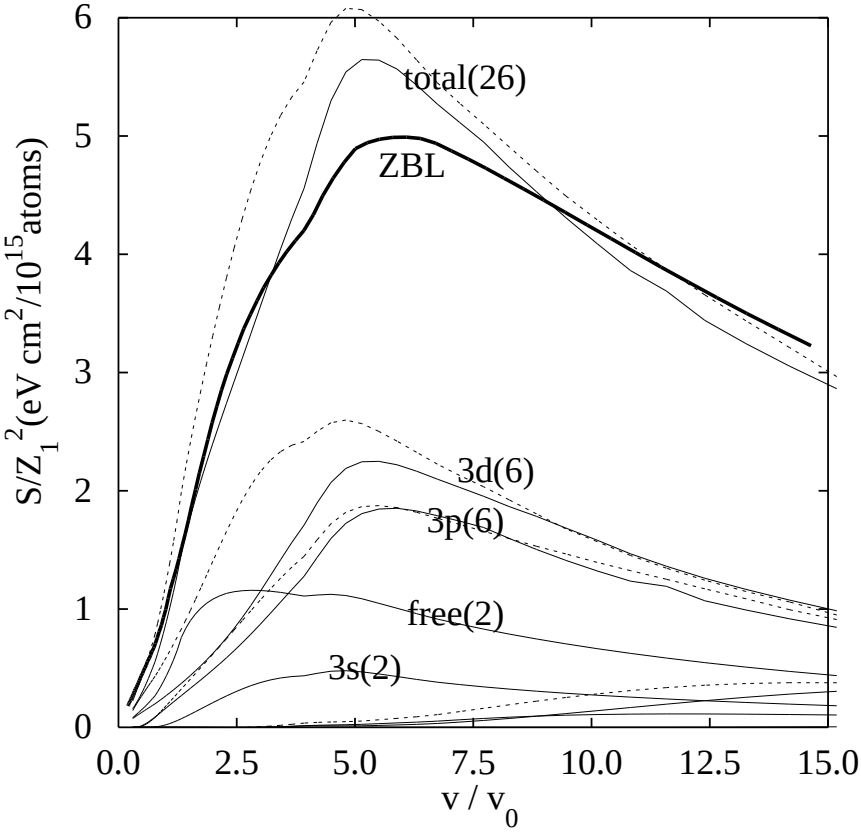

Figure 8: $_{15}$P stopping cross sections S and S_{shell} in $_{26}$Fe. Bold lines: ZBL [29]. Thin solid lines: Theory with the modified susceptibilities of p and d shells according to (22), appendix B and table 2. Dotted lines: Theory with the plain Gaussian (8) and the extended-basis values of table 1. All theoretical results used the dead sphere radius $r_c = 1.1\Lambda$ and the following cut energies E_{bnd} for Fe (in a.u.): 1s 261.12, 2s 31.68, 3s 3.911, 2p 27.15, 3p 2.484, 3d 0.3887, free none. Numbers in parentheses denote N_{shell}. The kinks at $v \approx 3.5v_0$ are an artifact imported from the variation of Λ in the ZBL ion model (fig. 6). Though the solid line of the 3p shell has been obtained with the $\bar{q}_1$ value of table 2, below that of table 1, the change from $l = 0$ to $l = 1$ in (21) has shifted the excitation spectrum to the right.

of the maximum of the fit $w(p)$ coincide with the wave number of the maximum of $|\varphi(p)|^2$:

$$p_m = \sqrt{l}\bar{q}_1 \qquad \text{if} \qquad l = 1, 2 \qquad . \tag{23}$$

Table 2 cites some values of $\bar{q}_1$ that are computed from a maximum search of $|\varphi(p)|^2$ of the extended basis set of the CR tables [3].

The six examples have larger characteristic wave numbers for the 2p shell, and lower for the 3p shell compared with the values of table 1. Fig. 8 illustrates the influence of the new susceptibility on the p and d subshell and total cross section of an $_{26}$Fe target.

Even though we have chosen (i) a target with a large number of electrons in p and d shells and (ii) a heavy ion with its stopping maximum fixed by the maxima of these subshell stopping powers, the total effect of the modified ground state momentum distribution on the stopping power is much less than one might have expected. The reduction of the target polarization as a whole can be interpreted by the broader distribution of electrons in the wall-type ansatz (21). The phase space available to the scattered electrons in the intermediate state has been effectively reduced compared with the Gaussian ansatz (8).

6 Summary

Effective-charge theory is the most general and practical ansatz of heavy-ion electronic stopping in random targets. The current implementations incorporate the major information on the target polarization by using experimental proton stopping data in the heavy ion scaling rule, and give no answer, whether the effective charge fraction may

be estimated from a free-electron target model. To lead to an improved understanding of the role of the inner-shell target electrons in the electronic stopping, we referred to the target model of Kaneko, which has been demonstrated before to predict light ion stopping cross sections successfully. In a first modification we introduced energy cuts in the energy loss functions for further improvement.

We turned to the incorporation of heavy ions in the Kaneko theory, aiming to calculate heavy ion stopping powers directly without recourse to the scaling rule. Our work explains how the increasing overestimation of the theory when increasing the ion atomic number may be understood as a wrong accounting of the target polarization at the ion place in the standard formula. We introduced a model to let the ion move rather *through* than *across* the target electrons, and could reduce this systematic error.

Eventually, based on a more selective description of the target electrons in p and d shells, new formulas for their polarization are proposed here. Their influence on the total stopping cross sections remains small.

Our more ab initio explanation of heavy ion stoppings does not compute effective charge fractions as a provisional result. But nevertheless, it is an effective-charge theory, as the conversion of the true ion charge into some effective charge with respect to the stopping is still provided by the mixture of close and distant collisions with the target electrons.

A Stopping Power Including a Dead Sphere

The region of the integration in (20) may be split by subtracting the dead sphere from the total space. The Fourier representation (1) and (2) are inserted

$$\Phi_{ind}(\mathbf{r},t) = \frac{1}{4\pi\epsilon_0}\left[\int d^3r' - \int_{|\mathbf{r}'-\mathbf{v}t|<r_c} d^3r'\right]\int \frac{d^3k d\omega}{(2\pi)^3} e^{i(\mathbf{k}\mathbf{r}'-\omega t)}\left[\frac{1}{\epsilon(\mathbf{k},\omega)}-1\right]\rho_m(\mathbf{k})\delta(\omega-\mathbf{k}\mathbf{v}) \quad .$$

This real space representation is inserted into the stopping power (3)

$$\int d^3r\,\rho_m(\mathbf{r},t)\mathbf{E}_{ind}(\mathbf{r},t)\mathbf{v} = -i\int \frac{d^3k'}{(2\pi)^3}\rho_m(-\mathbf{k}')e^{i\mathbf{k}'\mathbf{v}t}\mathbf{k}'\mathbf{v}\int d^3r\,e^{-i\mathbf{k}'\mathbf{r}}\Phi_{ind}(\mathbf{r},t) \quad .$$

Using $\int d^3r\, e^{i\tilde{\mathbf{k}}\mathbf{r}}/|\mathbf{r}-\mathbf{r}'| = 4\pi\, e^{i\tilde{\mathbf{k}}\mathbf{r}'}/\tilde{\mathbf{k}}^2$ we arrive at

$$\frac{dE}{dx} = \frac{dE}{dx}_{|r_c=0} + \frac{i}{v\epsilon_0}\int \frac{d^3k'}{(2\pi)^3}\rho_m(-\mathbf{k}')\frac{\mathbf{k}'\mathbf{v}}{\mathbf{k}'^2}\int\frac{d^3kd\omega}{(2\pi)^3}\left[\frac{1}{\epsilon(\mathbf{k},\omega)}-1\right]\rho_m(\mathbf{k})\delta(\omega-\mathbf{k}\mathbf{v})\int_{r'<r_c} d^3r'\,e^{i(\mathbf{k}-\mathbf{k}')\mathbf{r}'}.$$

Switching to spherical coordinates with some obvious notations like

$$\mathbf{k}'\mathbf{r}' = k'r'\left[\sin\theta_{r'}\sin\theta_{k'}\cos(\varphi_{r'}-\varphi_{k'}) + \cos\theta_{r'}\cos\theta_{k'}\right]$$

replaces the $\varphi_{k'}$ integral by a Bessel function [7, 8.411.7]

$$\int_0^{2\pi} e^{-ik'r'\sin\theta_{r'}\sin\theta_{k'}\cos(\varphi_{r'}-\varphi_{k'})}d\varphi_{k'} = 2\pi J_0(k'r'\sin\theta_{r'}\sin\theta_{k'}) \quad .$$

Using the same type of formula for the $\varphi_{r'}$ integration and $\rho_m(-\mathbf{k}') = \rho_m^*(\mathbf{k}')$ yields

$$\begin{aligned}\frac{dE}{dx} = \frac{dE}{dx}_{|r_c=0} &+ \frac{i}{v\epsilon_0(2\pi)^3}\int_0^\infty dk'\rho_m^*(k')k'\int_0^\pi \cos\theta_{k'}\sin\theta_{k'}d\theta_{k'}J_0(k'r\sin\theta_r\sin\theta_{k'})e^{-ik'r\cos\theta_r\cos\theta_{k'}}\\ &\times\int_0^\infty kdk\int_{-kv}^{kv}d\omega\left[\frac{1}{\epsilon(\mathbf{k},\omega)}-1\right]\rho_m(k)\int_0^{r_c} r^2\,dr\int_0^\pi \sin\theta_r d\theta_r J_0(kr\sqrt{1-\frac{\omega^2}{k^2v^2}}\sin\theta_r)e^{ikr\frac{\omega}{kv}\cos\theta_r} \quad .\end{aligned}$$

Some convolution of integration intervals may be done:

$$\int_0^\pi J_0(k'r\sin\theta_r\sin\theta_{k'})e^{i(k'r\cos\theta_{k'}-r\frac{\omega}{v})\cos\theta_r}\sin\theta_r d\theta_r J_0(r\sqrt{k^2-\frac{\omega^2}{v^2}}\sin\theta_r)$$

$$= 2\int_0^{\pi/2} J_0(k'r\sin\theta_r\sin\theta_{k'})\cos\left[(k'r\cos\theta_{k'} - r\frac{\omega}{v})\cos\theta_r\right]\sin\theta_r J_0(r\sqrt{k^2-\frac{\omega^2}{v^2}}\sin\theta_r)d\theta_r\,,$$

$$\int_0^{\pi}\cos\theta_{k'}\sin\theta_{k'}d\theta_{k'}J_0(k'r\sin\theta_r\sin\theta_{k'})\cos\left[(k'r\cos\theta_{k'} - r\frac{\omega}{v})\cos\theta_r\right]$$

$$= 2\int_0^{\pi/2}\cos\theta_{k'}\sin\theta_{k'}d\theta_{k'}J_0(k'r\sin\theta_r\sin\theta_{k'})\sin(k'r\cos\theta_{k'}\cos\theta_r)\sin(r\frac{\omega}{v}\cos\theta_r)\,. \qquad (24)$$

The $\theta_{k'}$ and afterwards the θ_r integrals have forms manageable by [7, 6.738], and create Spherical Bessel functions j_1

$$\int_0^{\pi/2}\sin\vartheta\cos\vartheta\sin(a\cos\vartheta)J_0(ab\sin\vartheta)d\vartheta = \frac{1}{(ab)^2}\int_0^{ab} u\,du\sin(\frac{1}{b}\sqrt{(ab)^2-u^2})J_0(u)du = \frac{1}{\sqrt{1+b^2}}j_1(a\sqrt{1+b^2})$$

$$\Rightarrow \frac{dE}{dx} = \frac{dE}{dx}_{|r_c=0} - \frac{1}{\epsilon_0\pi^3v^2}\int_0^{\infty}dk'\rho_m^*(k')k'\int_0^{r_c}dr\,r^2j_1(k'r)\int_0^{\infty}dk\rho_m(k)j_1(rk)\int_0^{kv}\omega d\omega\Im\frac{1}{\epsilon(k,\omega)}\,.$$

[7, 5.54.1] provides the underivative of the r integral. The result is decomposed into partial fractions

$$r_c^2k'\frac{kj_1(k'r_c)j_0(kr_c) - k'j_0(k'r_c)j_1(kr_c)}{k'^2-k^2} = -\frac{\sin(kr_c)}{k^2r_c}\frac{\sin(k'r_c)}{k'} + \frac{\sin(k'-k)r_c}{2k(k'-k)} + \frac{\sin(k'+k)r_c}{2k(k'+k)}\,.$$

The remaining 3-fold integral may be reduced to a double integral, if we restrict to the BK form factor (19). In this case, the law of residues yields

$$\int_0^{\infty}\rho_m(k')\left[\frac{\sin(k'+k)r_c}{k'+k} + \frac{\sin(k'-k)r_c}{k'-k}\right]dk' = Z_1e\Im\int_{-\infty}^{\infty}\frac{q+(k'\Lambda)^2}{1+(k'\Lambda)^2}\frac{e^{i(k'+k)r_c}}{k'+k}dk'$$

$$= \pi\left[Z_1e(q-1)e^{-r_c/\Lambda}\frac{k\Lambda\sin(kr_c)-\cos(kr_c)}{1+(k\Lambda)^2} + \rho_m(k)\right]\,. \qquad (25)$$

$$\frac{dE}{dx} = \frac{Z_1e}{2\epsilon_0v^2\pi^2}\int_0^{\infty}\frac{\rho_m(k)}{k}\left[\frac{(1-q)e^{-r_c/\Lambda}\{k\Lambda\sin kr_c - \cos kr_c\}}{1+(k\Lambda)^2} + \frac{\sin kr_c}{kr_c}\left\{q+(1-q)e^{-r_c/\Lambda}\right\}\right]dk$$

$$\times\int_0^{kv}\omega\Im\frac{1}{\epsilon(k,\omega)}d\omega\,. \qquad (26)$$

We may check that Z_1e times the term in the square brackets reduces to $\rho_m(k)$ in the limit $r_c \to 0$ and (26) becomes (4). This model of the polarization cut demands no additional numerical integration compared with (4).

B New Susceptibilities of p and d Shells

The RPA expression (9) with (21) inserted is written in cylinder coordinates with the axis in the direction of $\mathbf{k}$, $\mathbf{p} = \mathbf{p}_\parallel + \mathbf{p}_\perp, \mathbf{p}_\perp\mathbf{k} = 0, \mathbf{p}_\parallel\mathbf{k} = \pm p_\parallel k$ and $\delta\left(\omega - \hbar(\mathbf{p}+\mathbf{k})^2/(2m) + \hbar\mathbf{p}^2/(2m)\right) = \frac{m}{\hbar k}\delta\left(m\omega/(\hbar k) - k/2 \pm p_\perp\right)$

$$\int d^3p\,\left[(\mathbf{p}+\mathbf{k})^{2l}e^{-(\mathbf{p}+\mathbf{k})^2/\bar{q}^2} - p^{2l}e^{-p^2/\bar{q}^2}\right]\delta\left(\omega - \frac{\hbar(\mathbf{p}+\mathbf{k})^2}{2m} + \frac{\hbar\mathbf{p}^2}{2m}\right)$$

$$= 2\pi\frac{m}{\hbar k}\int_0^{\infty}dp_\perp p_\perp\left[\left(\frac{m\omega}{\hbar k} - \frac{k}{2}\right)^2 + p_\perp^2 + k^2 + \frac{2m}{k}\left(\omega - \frac{\hbar k^2}{2m}\right)\right]^l e^{-\left[\left(\frac{m\omega}{\hbar k}+\frac{k}{2}\right)^2+p_\perp^2\right]/\bar{q}^2} - \left\{\frac{k}{2}\leftrightarrow -\frac{k}{2}\right\}\,.$$

The integrals are easily handled with [7, 3.416.2,3.416.3]

$$\Im\chi^R = \frac{\chi^2\pi}{8z^3}\begin{cases} c_0^2\left\{e^{-(u-z)^2} - (z\leftrightarrow -z)\right\} & ,l=0 \\ (c_1\bar{q})^2\left\{[1+(u-z)^2]e^{-(u-z)^2} - (z\leftrightarrow -z)\right\} & ,l=1 \\ (c_2\bar{q}^2)^2\left\{[2+2(u-z)^2+(u-z)^4]e^{-(u-z)^2} - (z\leftrightarrow -z)\right\} & ,l=2 \end{cases}$$

The KK analysis (11) must evaluate integrals like

$$\int_{-\infty}^{\infty} \frac{(u \pm z)^{2l} e^{-(u\pm z)^2}}{u' - u} du = \int_{-\infty}^{\infty} \frac{t^{2l} e^{-t^2}}{u' \pm z - t} dt \,.$$

It may use the formula for the Hilbert transform of the first moment of a function given in [4, chapt. 15.1], starting with the integral [9]

$$\frac{P}{\pi} \int_{-\infty}^{\infty} dt \frac{e^{-t^2}}{t - x} = -\frac{2x}{\sqrt{\pi}} e^{-x^2} \, {}_1F_1(\frac{1}{2}, \frac{3}{2}; x^2) \equiv -\frac{2}{\sqrt{\pi}} G(x)$$

as an 'anchor' to calculate

$$\frac{P}{\pi} \int_{-\infty}^{\infty} dt \frac{te^{-t^2}}{t - x} = -\frac{2}{\sqrt{\pi}} xG(x) + \frac{1}{\pi} \int_{-\infty}^{\infty} e^{-t^2} dt = -\frac{2}{\sqrt{\pi}} xG(x) + \frac{1}{\sqrt{\pi}}$$

$$\frac{P}{\pi} \int_{-\infty}^{\infty} dt \frac{t^2 e^{-t^2}}{t - x} = \frac{x}{\sqrt{\pi}} \left(1 - 2xG(x)\right) \qquad ; \qquad \frac{P}{\pi} \int_{-\infty}^{\infty} dt \frac{t^3 e^{-t^2}}{t - x} = \frac{x^2}{\sqrt{\pi}} \left(1 - 2xG(x)\right) + \frac{1}{2\sqrt{\pi}}$$

and yield

$$\Re\chi^R = \frac{\chi^2\sqrt{\pi}}{8z^3} \begin{cases} 2c_0^2 \left\{G(u-z) - (z \leftrightarrow -z)\right\} & , l = 0 \\ (c_1\bar{q})^2 \left\{2\left[1 + (u-z)^2\right] G(u-z) - (u-z) - (z \leftrightarrow -z)\right\} & , l = 1 \\ (c_2\bar{q}^2)^2 \left\{-\frac{5}{2}(u-z) - (u-z)^3 + 2\left[2 + 2(u-z)^2 + (u-z)^4\right] G(u-z) - (z \leftrightarrow -z)\right\} & , l = 2 \end{cases}$$

References

1 Belkić D., H. S. Taylor, Physica Scripta 39 (1989) 226–9

2 Brandt W., M. Kitagawa, Phys. Rev. B 25 (9) (1982) 5631–7. The power of the factor (3/5) after (11) should read 7/3. Additional Errata Phys. Rev. B 26 (7) (1982) 3968

3 Clementi E., C. Roetti, Atom. Data Nucl. Data Tabl. 14 (3–4) (1974) 177–478

4 Erdély A. (editor), *Tables of Integral Transforms*, Vol. II of the *Batman Manuscript Project*, McGraw Hill, New York, Toronto, London, 1954

5 Ferell T. L., R. H. Ritchie, Phys. Rev. B 16 (1) (1977) 115–23

6 Golser R., D. Semrad, Phys. Rev. Lett. 66 (14) (1991) 1831–3

7 Gradstein I., I. Ryzhik, *Summen-, Produkt- und Integraltafeln*, Harri Deutsch (Thun) 1981, ISBN 3 87144 350 6

8 Kaneko T., Nucl. Instr. Meth. B 33 (1988) 147–50. The x in (3) should read χ. Table 1 has been updated by [10].

9 Kaneko T., Phys. Rev. A 40 (4)(1989) 2188–91; phys. stat. sol. (b) 156 (1989) 49–63. The factor 2 in the denominator of (2.12) should read 4. The rhs of (2.15) should be multiplied with 4π (CGS units) and the lhs of (2.22) with -1. A square is missing in the exponential of the denominator of (2.27).

10 Kaneko T., Atom. Data Nucl. Data Tabl. 53 (2) (1993) 271–340

11 Kaneko T., Nucl. Instr. Methods B 90 (1–4) (1994) 58–61

12 Kaneko T., H. Tuschida, J. Phys. B: At. Mol. Opt. Phys. 27 (1) (1994) 97–109

13 Lindhard J., Dan. Mat. Fys. Medd. 28, no. 8 (1954) 1–57

14 Lindhard J., A. Winther, Mat. Fys. Medd. Dan. Vid. Selsk. 34 (4) (1964) 1 – 22. The term $\chi^2/3$ in (15) should be preceded by minus both times.

15 Ma T.-C., Y.-N. Wang, T. Cui, J. Appl. Phys. 72 (8) (1992) 3838–40

16 Mann A., W. Brandt, Phys. Rev. B 24 (9) (1981) 4999–5002. The constants c_1 and c_2 in (9) should be interchanged.

17 Mathar R. J., M. Posselt, Phys. Rev. B1 (in press)

18 McLean A. D., R. S. McLean, Atom. Data Nucl. Data Tables 26 (3/4) (1981) 197–381

19 Nagy I., J. Phys. B: At. Mol. Phys. 19 (1986) L421–5

20 Nagy I., A. Arnau, P. M. Echenique, Phys. Rev. A 40 (2) (1989) 987–94

21 Pitarke J. M., R. H. Ritchie, P. M. Echenique, Nucl. Instr. Meth. B79 (1993) 209–12

22 Pitarke J. M., R. H. Ritchie, P. M. Echenique, Nucl. Instr. Methods B 90 (1994) 358–62

23 Sayasov Yu. S., N. A. Tahir, Europhys. Lett. 23 (9) (1993) 641–6

24 Stahl A., I. Balslev, *Electrodynamics of the Semiconductor Band Edge*, Vol. 110 of *Springer Tracts in Mod. Phys.*, Springer, Berlin, Heidelberg, 1987, ISBN 3-540-16953-9

25 Sung C. C., R. H. Ritchie, Phys. Rev. A 28 (2) (1983) 674–81

26 Valdés J. E., J. C. Eckardt, G. H. Lantschner, N. R. Arista, Phys. Rev. A 49 (2) (1994) 1083–8

27 Xia Y., C. Tan, W. N. Lennard, Nucl. Instr. Methods B 90 (1–4) (1994) 41–4 and 88–91

28 Yarlagadda B. S., J. E. Robinson, W. Brandt, Phys. Rev. B 17 (9) (1978) 3473–83

29 Ziegler J. F., J. P. Biersack, U. Littmark, Vol. 1 of *The Stopping and Range of Ions in Solids*, Pergamon Press (New York, Oxford, Toronto, ...) 1985, ISBN 0-08-021603-X. A factor of a is missing two times in (3-29).

30 Ziegler J. F., *Ion Implantation Physics*, pp 1–68 in *Handbook of Ion Implantation Technology, 1. Ion bombardment*, North-Holland (Amsterdam, London, New York, Tokyo), 1992 ed.: J. F. Ziegler, ISBN 0-444-89735-6

31 Ziegler J. F., J. M. Manoyan, Nucl. Instr. Meth. B 35 (1988) 215–28. The factor C_2 in (4) should read 0.48.